
Many-body effects beyond excitons in second-harmonic generation of monolayer MoS₂

Peio Garcia-Goiricelaya^{1*} and Julen Ibañez-Azpiroz^{2,3,4†}

¹ Department of Physics, University of the Basque Country UPV/EHU, 48940 Leioa, Basque Country, Spain

² Centro de Física de Materiales, Universidad del País Vasco UPV/EHU, 20018 Donostia-San Sebastián, Spain

³ Ikerbasque Foundation, 48013 Bilbao, Spain

⁴ Donostia International Physics Center, 20018 Donostia-San Sebastián, Spain

* peio.garcia@ehu.eus, † julen.ibanez@ehu.eus

Abstract

We present a quantitative study of many-body effects including the three-particle level on second-harmonic generation in monolayer MoS₂. Our approach combines many-body perturbation theory with time-dependent current-density-functional theory within an *ab initio* framework in the optical limit. The inclusion of two-particle excitonic effects via a dynamical long-range linear exchange–correlation kernel reproduces the qualitative features of the second-harmonic response, but underestimates the experimentally reported magnitude by nearly a factor of two. By incorporating three-particle trionic correlations through a static long-range quadratic exchange-correlation kernel, we achieve significantly improved quantitative agreement with experiment. These findings highlight the role of many-body interactions beyond the excitonic level in accurately describing second-order optical responses in two-dimensional semiconductors.

Contents

1	Introduction	2
2	Theoretical framework	4
2.1	Tensorial many-body description of second-harmonic generation	4
2.2	Modeling monolayer MoS ₂	4
3	Electronic band structure and linear optical response	5
4	Two- and three-body effects on second-harmonic generation	7
5	Conclusions and Outlook	8
A	Computational details	9
B	Connection between TDDFT and TDCDFT	10
B.1	Time-dependent density functional theory	10
B.2	Time-dependent current-density functional theory	11
B.3	TDCDFT in the optical and long-wavelength limit	12

1 Introduction

Nonlinear optics encompasses physical phenomena in which the response of materials to incident light is not linearly proportional to the field amplitude [1]. Unlike the linear regime, nonlinear optical processes enable the generation of light at modified frequencies, for instance, through second-harmonic generation (SHG) [2]. The last decade has witnessed a growing interest in higher-order optical responses for their technological potential. A notable example is the bulk photovoltaic effect (BPVE) that occurs in noncentrosymmetric crystals [3], investigated as a promising mechanism for direct current generation beyond conventional solar cells [4]. Similarly, nonlinear optical effects in topological materials have gained significant interest [5–9] due to their deep connection with topological Berry-phase-like quantities [10].

A robust and predictive theoretical understanding of nonlinear optics is therefore highly desirable for the development of emerging optical technologies [11]. In this context, first principles calculations based on density functional theory (DFT) play a central role, providing microscopic and system-specific insights [12–17]. However, achieving quantitative accuracy requires the explicit incorporation of many-body interactions into these theoretical frameworks [18]. This is particularly important in low-dimensional semiconducting systems, where reduced electronic screening amplifies many-particle correlated effects [19]. The emergence of collective excitations often dominates the optical response of such nanostructured materials, which have rapidly become leading platforms for future technological applications [20].

A clear view of the role of many-body interactions in nonlinear optical responses can be obtained within the framework of time-dependent DFT (TDDFT) [21]. In this formalism, the interacting quadratic density response function is expressed through a Dyson-like shorthand equation as [22]

$$\chi_{\rho 2} = \varepsilon^{-1} \chi_{\rho 2}^0 \varepsilon^{-1} \varepsilon^{-1} + \chi_{\rho 1} g_{xc} \chi_{\rho 1} \chi_{\rho 1}, \quad (1)$$

where the linear contribution is

$$\chi_{\rho 1} = \chi_{\rho 1}^0 \varepsilon^{-1}, \quad (2)$$

with $\varepsilon^{-1} = 1 + (v_c + f_{xc})\chi_{\rho 1}$ the inverse of the dielectric function and v_c the Coulomb interaction, *i.e.* the functional derivative of the Hartree potential with respect to density. Above, $\chi_{\rho n}$ and $\chi_{\rho n}^0$ denote the many-body (interacting) and independent-particle (non-interacting) density response functions at n -th order, respectively. In turn, f_{xc} and g_{xc} are the *unknown* linear and quadratic exchange-correlation (xc) kernels, *i.e.* the first and second functional derivatives of the xc potential with respect to density, respectively. As seen by the equations above, these terms drive the many-body renormalization of linear and quadratic optical responses and are therefore the primary focus of this study.

From a many-body perturbation theory (MBPT) perspective, Eqs. (2) and (1) are formally equivalent to contracting the correlation parts of the two- and three-particle Green's functions, respectively [23]. Importantly, this establishes a correspondence between the two- and three-body interactions and the linear f_{xc} and quadratic g_{xc} xc kernels of TDDFT, respectively. Thus, when evaluating the response to light, f_{xc} encapsulates electron-hole interactions, as schematically illustrated in Fig. 1(a), leading to the formation of two-particle bound states, or *excitons* [24, 25]. In turn, g_{xc} incorporates electron-electron-hole and electron-hole-hole

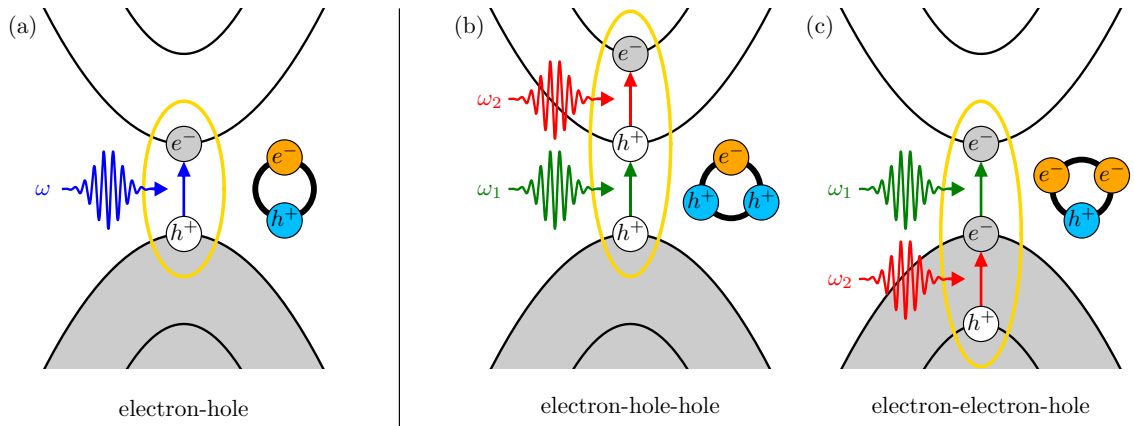


Figure 1: Schematic of two-particle (a) and three-particle (b,c) many-body interactions in the linear and quadratic optical response of a semiconductor, respectively. Grey and white shaded lines represent valence and conduction bands, respectively.

interactions depicted in Figs. 1(b) and (c), respectively. The associated composite quasiparticles, known as *trions* or charged excitons, are three-particle bound states that emerge from neutral excitons upon carrier doping [26, 27].

The most direct way of computing nonlinear optical responses beyond the independent-particle approximation is to evaluate the response functions explicitly in terms of many-body wavefunctions and energies. Over the past two decades, such calculations have been extensively carried out at second order using a basis of two-particle excitonic states [28–42], while systematically neglecting three-particle trionic contributions. In parallel, state-of-the-art TDDFT approaches typically start from a quasiparticle-corrected independent-particle response and incorporate excitonic effects through long-range approximate forms of the linear xc kernel, whereas trionic effects encased in the quadratic xc kernel are always omitted [43–48]. As evident from Eq. (1), this leads to a partially interacting second-order response that accounts only for two-particle correlations, again excluding three-particle contributions. This constitutes a significant limitation: just as the two-body electron-hole interaction is essential for describing linear optical absorption, nonlinear optical responses are likewise expected to be increasingly governed by many-body interactions beyond the two-particle level.

In this work, we investigate the influence of many-body interactions including the three-particle level on SHG. We have selected monolayer MoS_2 as a case study for two main reasons. First, its reduced dimensionality gives rise to pronounced many-body excitonic [49–53] and trionic [54, 55] signatures in optical absorption and photoluminescence spectra. Second, this material, as well as similar transition-metal dichalcogenide compounds, have recently shown signatures of remarkable nonlinear optical processes [56–58]. Our main result shows that including quadratic xc contributions that account for trionic effects leads to an improved quantitative agreement with experimental SHG spectra, emphasizing the important role of three-body interactions in accurately modeling second-order photoresponses.

The paper is organized as follows. In Sec. 2, we present the main theoretical framework. We first introduce the second-harmonic generation tensor renormalized by many-body interactions. We then describe in detail the modeling of monolayer MoS_2 . In Secs. 3 and 4, we present and analyze the numerical results for the linear and quadratic optical regimes, respectively. We conclude in Sec. 5 with a summary and discussion. In Appendices A and B we provide the computational details of the calculations and describe our theoretical methodology.

2 Theoretical framework

2.1 Tensorial many-body description of second-harmonic generation

Eqs. (2) and (1) describe the interacting linear and quadratic responses within TDDFT, respectively. Although formally appealing, their scalar formulation makes it cumbersome to resolve directional components of the response, which are more naturally captured within a tensorial framework. To this end, we employ time-dependent current-density functional theory (TDCDFT) [59, 60]. This formalism represents the tensorial extension of TDDFT, in which the charge density and scalar potentials are replaced by the current density and electric fields, and the scalar response functions and xc kernels by their tensorial counterparts. In addition, TDCDFT allows the response equations to be formulated without long-wavelength divergences in the optical limit and without divergences at zero frequency in the static limit. Details of the connection between the two frameworks are provided in Appendix B.

In this work, we focus on SHG, *i.e.* the quadratic optical process in which two photons of frequency ω are absorbed to generate radiation at frequency 2ω , corresponding to $\omega_1 = \omega_2 = \omega$ in Figs. 1(b) and (c). In this case, the interacting quadratic optical response at the microscopic level can be expressed in terms of polarizability tensors as [48]

$$\alpha_2(\omega, \omega) = \boldsymbol{\varepsilon}^{-1,T}(2\omega)\alpha_2^0(\omega, \omega)\boldsymbol{\varepsilon}^{-1}(\omega)\boldsymbol{\varepsilon}^{-1}(\omega) + i\alpha_1^T(2\omega)\mathbf{B}_{\text{LRC}}(\omega, \omega)\alpha_1(\omega)\alpha_1(\omega), \quad (3)$$

where the linear contribution is given by

$$\alpha_1(\omega) = \alpha_1^0(\omega)\boldsymbol{\varepsilon}^{-1}(\omega), \quad (4)$$

with

$$\boldsymbol{\varepsilon}^{-1}(\omega) = \mathbb{1} - [4\pi - \mathbf{A}_{\text{LRC}}(\omega)]\alpha_1(\omega), \quad (5)$$

which defines the inverse of the optical dielectric tensor. Above, α_n and α_n^0 are the many-body and independent-particle optical polarizability tensors at n -th order, respectively. In Eq. (3), two-body excitonic effects enter through the optical dielectric tensor *via* \mathbf{A}_{LRC} , while three-body trionic effects are encoded in \mathbf{B}_{LRC} . These quantities are material-dependent tensors that parameterize the strength of the long-range contributions (LRC) of the linear and quadratic xc kernels in the optical limit. Due to the space group $P\bar{6}m2$ and the point group D_{3h} of monolayer MoS_2 , the in-plane symmetry-allowed components of second- and third-rank tensors satisfy the equivalence relations $xx = yy$ and $xyx = yxy = yxx = -yyy$, respectively.

Our calculation strategy consists of several steps. Based on DFT calculations, we first include one-body electron–electron and two-body electron–hole interactions within MBPT using the *GW* approximation [61, 62] and the Bethe–Salpeter equation (BSE) [63], respectively. This yields an accurate macroscopic optical dielectric tensor [see Eq. (5)] that incorporates quasiparticle corrections and excitonic effects. From it, we extract the linear LRC screening tensor \mathbf{A}_{LRC} , which reproduces the interacting linear optical response [see Eq. (4)]. This tensor is then employed in state-of-the-art calculations of SHG using Eq. (3), where the quantitative impact of trionic effects is assessed by tuning the quadratic LRC screening tensor \mathbf{B}_{LRC} . Technical details of the calculations can be found in Appendix A.

2.2 Modeling monolayer MoS_2

To model monolayer MoS_2 , we considered a supercell (sc) with a hexagonal close-packed structure of two planes of sulfur atoms with an intercalated plane of molybdenum atoms. The in-plane lattice parameter is set equal to the experimental bulk value, *i.e.*, 3.16 \AA [64], and a supercell height of $L_{\text{sc}} = 20 \text{ \AA}$ is used in the out-of-plane direction, providing a sufficiently large

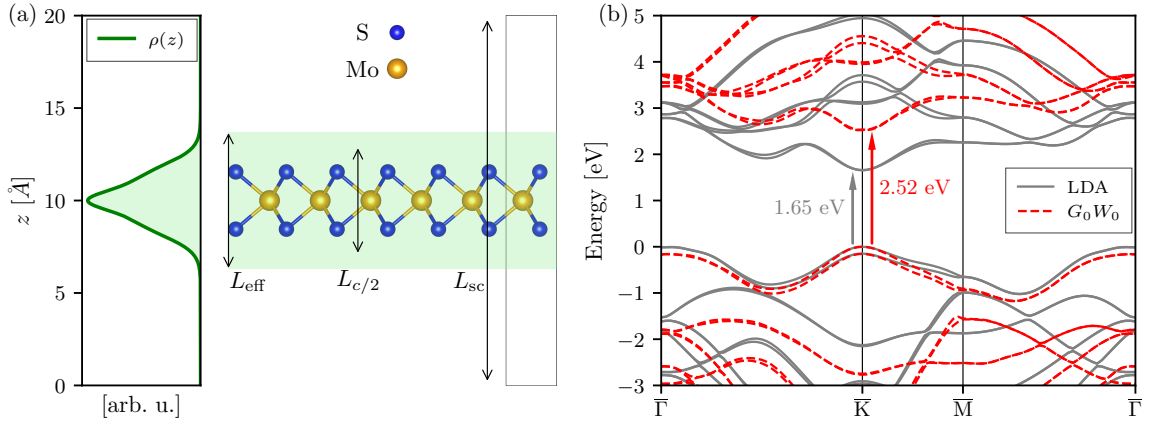


Figure 2: (a) Out-of-plane extension of the in-plane averaged charge density (left) together with the OYZ side view of the slab crystal unit (right) of monolayer MoS₂. Supercell thickness, effective thickness, and half of the bulk thickness are $L_{\text{sc}} = 20$ Å, $L_{\text{eff}} = 7.3$ Å and $L_{c/2} = 6.15$ Å [64], respectively. The green-shaded area highlights the effective out-of-plane spatial extent of the electrons. (b) LDA (solid grey lines) and G_0W_0 (dashed red lines) electronic band structure of monolayer MoS₂. LDA and G_0W_0 direct energy band gaps are equal to 1.65 eV and 2.52 eV, respectively.

vacuum region to avoid spurious interactions between periodic images. Spurious Coulomb interactions are further suppressed using the truncated scheme of Ref. [65]. The equilibrium atomic positions were determined by relaxing all atomic forces up to at least 10^{-6} Ry/ a_0 , leading to a relaxed interplanar distance equal to 1.55 Å, equivalent to a Mo-S bond length of 2.39 Å, in good agreement with previous theoretical calculations [66, 67].

Following a well-established procedure [68], the response tensors are rescaled from the supercell to the monolayer by the factor $L_{\text{sc}}/L_{\text{eff}}$, where L_{eff} is the effective monolayer thickness, yielding 3D-like quantities. We used a value of $L_{\text{eff}} = 7.3$ Å, obtained from the spatial extent of the charge density along the out-of-plane direction, as shown in Fig. 2(a). This value is in close agreement with the experimental atomic thickness of approximately 8 Å reported in the Supplemental Information of Ref. [56]. We note that the effective thickness employed here differs from the value $L_{c/2} = 6.15$ Å used in other works, which corresponds to half of the out-of-plane bulk lattice parameter [64] [see Fig. 2(a)].

3 Electronic band structure and linear optical response

We begin by inspecting the electronic band structure of monolayer MoS₂. The LDA calculation shown by solid grey lines in Fig. 2(b) predicts that the system is a semiconductor with a direct energy band gap of about 1.65 eV at high symmetry point \bar{K} . In order to improve this description, we include quasiparticle corrections to the band structure by approximating self-energy effects of single-particle excitations arising from electron–electron interactions within the one-shot G_0W_0 approximation. The resulting quasiparticle band dispersion is illustrated by the dashed red lines in Fig. 2(b), which predicts a direct band gap of 2.52 eV, much closer to the experimentally reported value of ~ 2.34 eV [70].

We next focus on the linear optical response. In order to capture excitonic effects of two-particle excitations arising from electron-hole interactions, we solve BSE to obtain the macroscopic optical dielectric spectrum. In Fig. 3(a), we compare this quantity as calculated within the G_0W_0 and BSE approaches, shown by the narrow red and broad blue lines, re-

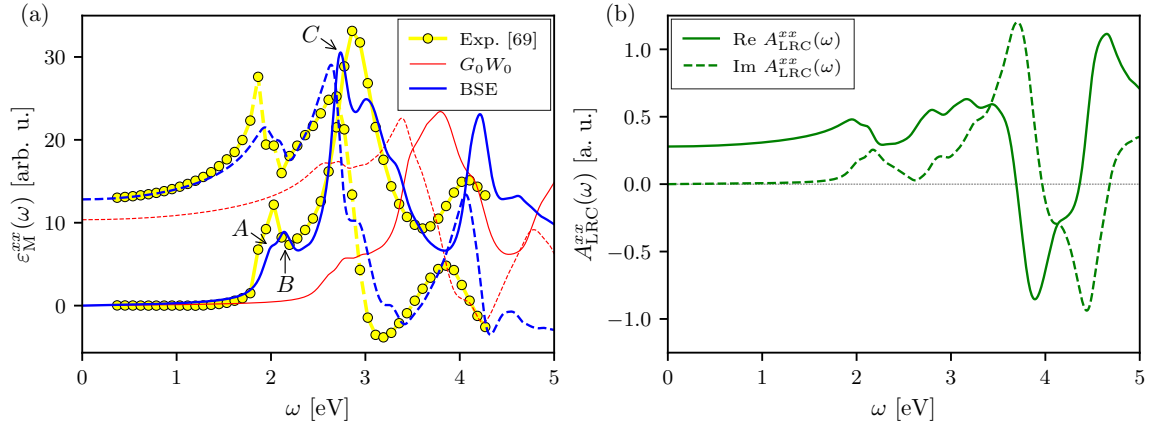


Figure 3: (a) Macroscopic optical dielectric spectrum of MoS₂. Dashed and solid yellow lines with circles represent the real and imaginary parts of experimental data, respectively, from Ref. [69]. Dashed and solid narrow red (broad blue) lines represent the real and imaginary parts within the G_0W_0 (BSE) picture, respectively. (b) In-plane component of the linear LRC screening tensor $A_{\text{LRC}}(\omega)$. Solid and dashed green lines represent the real and imaginary parts, respectively.

spectively. The BSE results exhibit very good agreement with experimental data [69], shown by yellow lines with circles, and clearly improved upon the G_0W_0 spectrum by incorporating two-body excitonic effects. Indeed, the BSE optical spectrum captures the spin-split A and B exciton double-peak structure between 2 and 2.15 eV, followed by the C peak around 2.7 eV. All these results are in good agreement with previous DFT plus MBPT calculations [49–53].

Based on the BSE results shown in Fig. 3(a), we now proceed to construct a tensorial xc kernel in the linear regime that accounts for excitonic effects within TDCDFT. In the optical limit, the linear xc kernel of TDDFT is dominated by its long-range contribution and behaves *exactly* like an attractive screened Coulomb interaction that emulates the electron-hole attraction, in such a way that $\lim_{\mathbf{q} \rightarrow 0} f_{\text{xc}}(\mathbf{q}) = -A_{\text{LRC}}/q^2$, where \mathbf{q} is the crystal momentum transfer and the screening parameter A_{LRC} is an *unknown* material-dependent quantity [71, 72]. Empirical [73–75] and nonempirical [76–82] static evaluations of the linear LRC screening parameter have only proven to work well to some extent for *continuum* excitonic effects and at most one bound exciton peak, but fail to describe multiple excitonic features. On the other hand, a dynamical extension of this quantity has been shown to be essential in order to reproduce subtle excitonic features within TDDFT starting from very good evaluations of the macroscopic optical dielectric function that can be, for instance, the result of BSE [83, 84].

As for TDDFT, an expression can be derived for calculating the linear LRC screening tensor within TDCDFT in the optical limit, in such a way that

$$A_{\text{LRC}}(\omega) = -4\pi \{ [\boldsymbol{\epsilon}_{\text{BSE}}(\omega) - \mathbf{1}]^{-1} - [\boldsymbol{\epsilon}_{\text{RPA}}(\omega) - \mathbf{1}]^{-1} \}, \quad (6)$$

where $\boldsymbol{\epsilon}_{\text{RPA}}$ denotes the optical dielectric tensor in the random phase approximation (RPA), *i.e.* neglecting many-body interactions, and $\boldsymbol{\epsilon}_{\text{BSE}}$ the BSE optical dielectric tensor including excitonic effects. The in-plane component of the linear LRC screening tensor calculated in this way is shown in Fig. 3(b). The figure shows a rather intricate structure, with multiple peaks and dips in both the real and imaginary parts of $A_{\text{LRC}}^{xx}(\omega)$ in the excitonic frequency region. Importantly, this fine structure going beyond what can be achieved by simple approaches allows to incorporate the multiplex structure of excitons into TDCDFT.

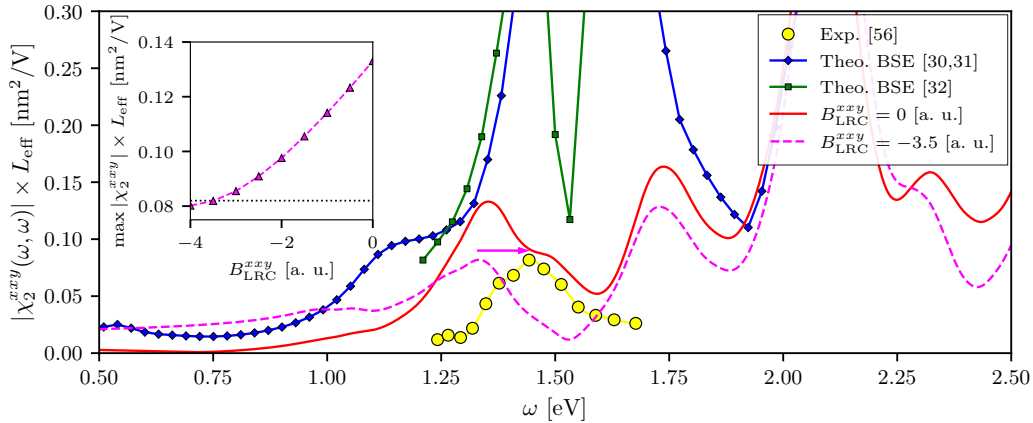


Figure 4: Absolute value of the macroscopic two-dimensional SHG susceptibility per unit area of monolayer MoS₂. The yellow line with circles dots represents experimental data from Ref. [56]. The blue line with diamonds and green line with squares represent theoretical results including excitonic effects at the BSE level from Refs. [30, 31] and [32], respectively. The solid red line represents our theoretical results including many-body interactions up to the two-particle level, *i.e.* excitonic effects with $B_{\text{LRC}}^{xy} = 0$ a.u., while the dashed magenta line includes also at the three-particle level, *i.e.* trionic effects with $B_{\text{LRC}}^{xy} = -3.5$ a.u.. Inset represents the theoretical value of the height of the peak close to 1.5 eV as a function of the in-plane longitudinal component of the quadratic LRC screening tensor B_{LRC}^{xy} with the dotted line being the experimental value.

4 Two- and three-body effects on second-harmonic generation

We are now in a position to address our central objective of calculating the macroscopic SHG susceptibility from first principles, which is obtained as a macroscopic average of the interacting SHG response at the microscopic level (see Appendix B.4). We evaluate the response by gradually turning on many-body interactions. In Fig. 4, we compare the calculated absolute value of the macroscopic SHG susceptibility obtained by including only excitonic effects at the two-particle level with $B_{\text{LRC}} = 0$ a.u. (solid red line) with theoretical BSE results reported in the literature [30–32] (blue and green lines with squares and diamonds), as well as with available experimental data from Ref. [56] (yellow line with circles). The onset of the SHG signal occurs around 1 eV, coinciding with half the eigenvalues of the spin-split *A* and *B* bound excitons [see Fig. 3(a)]. The signal then reaches its first pronounced maximum through the strongly absorbing bound exciton *C* [see Fig. 3(a)], as half of its eigenvalue coincides with the energy of the corresponding SHG peak (see Fig. 4). Accordingly, our calculations predict a well-defined SHG resonance at 1.35 eV, which is in very good agreement with the experiment, showing a SHG peak slightly below 1.5 eV. Although previous theoretical works have captured this overall trend [30–32], our results additionally exhibit a remarkable quantitative agreement in the order of magnitude. In contrast, earlier studies required an empirical rescaling of their spectra to reproduce the experimental magnitude of the SHG response. This improvement arises from two main factors. First, Wannier interpolation allows for Brillouin zone sampling to be several orders of magnitude denser than those employed in previous works, significantly enhancing numerical convergence and accuracy. Second, we have adopted an effective layer thickness determined from the spatial extent of the charge density along the out-of-plane direction of the supercell, rather than the conventional choice of one half of the bulk lattice constant. This

definition is consistent with the experimentally measured atomic thickness [56] and provides a more physically grounded estimate.

Despite the substantial improvement over previous theoretical predictions, our SHG result for $B_{\text{LRC}} = 0$ a.u. still yields an intensity of approximately $0.14 \text{ nm}^2/\text{V}$, significantly above the experimental value of $0.08 \text{ nm}^2/\text{V}$. At this stage, our treatment has accounted for many-body interactions only up to the two-particle level, meaning that only the first term on the right-hand side (r.h.s.) of Eq. (3) has been considered in the evaluation of the interacting microscopic SHG response. However, it is the second term that accounts for many-body effects at the three-particle level, which are themselves linearly screened, as the quadratic LRC screening tensor B_{LRC} correlates three interacting linear optical responses. Therefore, it is reasonable to expect that if an effect is large at first order, it will also manifest prominently at second order. This idea contradicts the common approximation in the literature of disregarding the quadratic xc kernel [43–48].

In our formulation, we exploit the *exact* static behavior of the quadratic xc kernel of TDDFT in the optical limit, which has been previously derived from a second-order BSE for the three-particle correlation function by Hübener [23]. In this limit, the long-range contribution dominates, such that $\lim_{\mathbf{q} \rightarrow 0} g_{\text{xc}}(\mathbf{q}, \mathbf{q}) = B_{\text{LRC}}/q^3$ [23], where B_{LRC} is a material-dependent parameter. Unlike conventional (first-order) BSE, its second-order counterpart has not yet been implemented in practical calculations; therefore, the tensor B_{LRC} cannot be obtained in the same way as A_{LRC} . As a result, no previous studies appear to have addressed its explicit evaluation. Nevertheless, by comparing experimental spectra with theoretical results that include many-body effects only up to the two-particle level, a reasonable range of values for B_{LRC} can be inferred, as we do next.

We proceed by comparing the maximum SHG peak intensity from our theoretical predictions with the experimental value as a function of the in-plane component of B_{LRC} . The results are shown in the inset of Fig. 4, indicating that for values $B_{\text{LRC}}^{\text{xy}} \in [-4, 0]$ a.u., the impact on the maximum SHG response is significant, reducing it by nearly a factor of two. In particular, theoretical results match the experimental peak intensity for $B_{\text{LRC}}^{\text{xy}} = -3.5$ a.u., from which we identify this value as optimal for the quadratic LRC screening parameter. The corresponding SHG spectrum is shown in main Fig. 4 (dashed magenta line). Besides the peak intensity, the shape of the main SHG peak at 1.4 eV is very well captured by our calculations, with only a ~ 0.1 eV energy redshift of our computed result compared to the experiment, a discrepancy that lies within the typical uncertainty of *GW* and BSE calculations within the MBPT framework. This result demonstrates that three-particle correlations can be comparable in magnitude to two-particle contributions and are therefore indispensable for quantitative theoretical predictions of nonlinear optical responses, such as SHG. This should not come as a surprise, given that experimental reports consistently indicate that trionic effects play a significant role in these types of two-dimensional materials [54, 55].

5 Conclusions and Outlook

In summary, our *ab initio* results demonstrate that many-body interactions beyond the usual two-particle excitation level are necessary for a quantitative description of the SHG spectrum in monolayer MoS_2 . By employing highly dense \mathbf{k} -point meshes enabled by the Wannier interpolation technique, our TDCDFT calculations, combined with a dynamical long-range linear xc kernel derived from the BSE, accurately capture the multiple excitonic structure as well as the order of magnitude of the SHG response. However, this is not sufficient to achieve quantitative agreement with experiment, with a discrepancy of nearly a factor of two in the intensity. By incorporating trionic effects through a static long-range quadratic xc kernel, we

bridge this gap and obtain excellent agreement with experiment in both peak positions and intensities. These findings reveal that three-body effects, which are almost universally neglected in standard theoretical treatments, can play an important role in second-order optical processes. More broadly, our work closes a quantitative gap between theory and experiment for SHG in low-dimensional semiconductors and establishes a framework for improved predictions of other quadratic optical responses in emerging materials.

Building on the present analysis of SHG, it is natural to ask what is the role of three-body interactions in other nonlinear optical responses. Among these, the shift- and injection-current contributions to the BPVE [3] are particularly compelling, given the significant attention this phenomenon has received in recent years. Such quadratic optical processes occur when the absorbed two photons have opposite energies, *i.e.* $\omega_1 = \omega = -\omega_2$ [see Figs. 1(b,c)]. Adapting Eq. B.18 from Appendix B to these processes, the Dyson-like expression in the frequency domain that accounts for such interacting optical conductivity tensors at the microscopic level within TDCDFT reads as [48]

$$\sigma_2(\omega, -\omega) = \epsilon^{-1T}(0)\sigma_2^0(\omega, -\omega)\epsilon^{-1}(\omega)\epsilon^{-1}(-\omega) + i\sigma_1^T(0)\frac{B_{\text{LRC}}(\omega, -\omega)}{\omega^2}\sigma_1(\omega)\sigma_1(-\omega), \quad (7)$$

where σ_n and σ_n^0 are the many-body and independent-particle conductivity tensors at n -th order. By inspecting Eq. 7, we note that in semiconductors of practical interest with a finite band gap, the first term on the r.h.s. can be non zero, whereas the second term will always vanish. This follows from the fact that, in undoped semiconductors, the lineal conductivity in the static limit is zero, that is, $\sigma_1(0) = 0$. As a result, when analyzing the shift- and injection-current contributions to BPVE, many-body effects enter only by means of the first term, thus limited to the two-particle excitonic level. In this way, previous calculations based on excitonic wavefunctions and energies can be regarded as formally consistent in their treatment of many-body interactions [36–42]. However, this result appears to be rather specific, owing to the direct current (DC) nature of BPVE, which manifests through the DC term $\sigma_1(0)$ in Eq. (7). In general, three-particle correlations to quadratic responses cannot be expected to vanish; therefore, theoretical frameworks such as the present one that explicitly include them are necessary.

Acknowledgements

The authors are grateful to Alejandro Molina-Sánchez for helpful discussions related with GW & BSE calculations as well as guidance using the YAMBO code. The authors acknowledge financial support of the European Union’s Horizon 2020 research and innovation programme under the European Research Council (ERC) grant agreement No. 946629, and the Spanish Ministry of Science, Innovation and Universities (MICIU) under the “Proyectos de Generación de Conocimiento” grant No. PID2023-147324NA-I00.

A Computational details

We performed ground-state electronic structure calculations using density functional theory (DFT) [85, 86] in the local density approximation (LDA) [87] as implemented in the QUANTUM ESPRESSO code package [88–90]. The interaction between valence electrons and atomic cores was modeled by means of norm-conserving pseudopotentials [91, 92] from the optimized norm-conserving Vanderbilt SG15 pseudopotentials database [93, 94] including fully relativistic corrections [95]. In the case of molybdenum, besides 4d and 5s valence electrons, 4s and 4p

semi-core electrons were also explicitly included as valence states, since they are known to be crucial for proper self-energy calculations based on the GW method [50, 96]. Self-consistent DFT calculations were carried out using a \mathbf{k} -point mesh of 12×12 in combination with fixed occupation values and a plane-wave basis set with a cutoff energy of 100 Ry.

Starting from LDA wave functions and energies, we calculated quasiparticle (QP) corrections due to electron-electron interactions within the one-shot G_0W_0 approximation [61, 62] and, subsequently, linear optical absorption spectra including excitonic effects through BSE [63], as implemented in the YAMBO code package [97, 98]. Concerning G_0W_0 calculations, we selected the main parameters by focusing on the convergence of the QP band-gap energy, as well as the conduction-band minimum and valence-band maximum, with a threshold below 15 meV. We applied the plasmon-pole approximation [99–101] with an energy cutoff of 12 Ry and 40 Ry for the dielectric matrix and both the exchange and correlation parts of the self-energy, respectively, and we included up to 220 bands in the sum-over-states of the dielectric matrix and the correlation part of the self-energy. We obtained converged values for a \mathbf{k} -point mesh of 30×30 . To speed up the convergence with respect to empty states, we adopted the technique described in Ref. [102]. In addition, to accelerate convergences with respect to the \mathbf{k} -point sampling avoiding long-wavelength divergences of the electronic potential, we used the so-called random integration method of the screened potential (RIM-W) [103] together with the truncation of the Coulomb potential in the slab geometry. In this way, we performed Monte Carlo integrations with 2×10^6 random points taking into account \mathbf{G} vectors up to 2.5 Ry and 1 Ry for the bare and screened Coulomb potentials, respectively. For the BSE calculations, we employed the Lanczos-Haydock solver [104], since our interest lies in the excitonic optical spectrum rather than in storing the full excitonic wave functions. An energy cutoff of 25 Ry and 8 Ry is used for the electron-hole exchange and attraction parts, respectively, of the BSE kernel, and 14 occupied and 22 unoccupied states have been used to build up the excitonic Hamiltonian. We used a \mathbf{k} -point mesh of 33×33 , which is enough to provide a good convergence in the position of the excitonic peaks.

As a next step, we evaluated independent-particle SHG susceptibility tensors at LDA and G_0W_0 levels in the optical and long-wavelength limit. We considered the length-gauge expressions [68, 105–107] as implemented in the WANNIER90 code package [48, 108]. To this end, starting from a set of 48 spin-split bands, we constructed 36 disentangled maximally localized Wannier functions spanning the 14 high-energy valence bands and the 22 low-energy conduction bands using two p trial orbitals centered on S atoms, as well as one s and one d trial orbitals centered on the Mo atom. To obtain well-converged optical spectra, we used a dense \mathbf{k} -point interpolated mesh of 1000×1000 . With respect to the imaginary part of the complex $\hbar\tilde{\omega}$, we set $\eta = 0.1$ eV, consistent with photoexcited carrier lifetimes (~ 10 fs) [109]. Regarding the auxiliary parameter for regularizing energy denominators, we chose $\eta_r = 0.05$ eV. The occupation factors and their derivatives were evaluated at zero temperature ($T = 0$ K).

B Connection between TDDFT and TDCDFT

In this appendix, we review the main derivation steps for obtaining tractable microscopic response equations within TDCDFT in the optical limit starting from TDDFT. The connection between the macroscopic and microscopic levels of the response is also discussed.

B.1 Time-dependent density functional theory

In TDDFT, one investigates the density response of a many-body system of electrons interacting *via* the Coulomb interaction to an externally applied time-dependent potential. Alternatively, one can adopt the auxiliary independent-particle system of non-interacting electrons, where the

density response is now viewed with respect to the total time-dependent potential felt by the particles. For quadratic responses, this entails expanding the time-dependent density response of the interacting system in a power series of the external potential up to second order,

$$\rho(1) = \int_0^1 \chi_{\rho 1}(1, 2) V_{\text{ext}}(2) d2 + \int \int_0^1 \chi_{\rho 2}(1, 2, 3) V_{\text{ext}}(2) V_{\text{ext}}(3) d2 d3, \quad (\text{B.1})$$

or, in the non-interacting case, in a power series of the total potential,

$$\rho(1) = \int_0^1 \chi_{\rho 1}^0(1, 2) V_{\text{tot}}(2) d2 + \int \int_0^1 \chi_{\rho 2}^0(1, 2, 3) V_{\text{tot}}(2) V_{\text{tot}}(3) d2 d3, \quad (\text{B.2})$$

where $\chi_{\rho n}$ and $\chi_{\rho n}^0$ are the many-body and independent-particle density response functions and we adopted the notation $(\mathbf{r}_n, t_n) \equiv (n)$ with n a positive integer and with the total potential related to the external potential as

$$V_{\text{tot}}(\mathbf{r}, t) = V_{\text{ext}}(\mathbf{r}, t) + V_{\text{H}}(\mathbf{r}, t) + V_{\text{xc}}(\mathbf{r}, t). \quad (\text{B.3})$$

The Hartree potential as a function of the density response is given by

$$V_{\text{H}}(1) = \int_0^1 v_{\text{c}}(1, 2) \rho(2) d2, \quad (\text{B.4})$$

with the Coulomb interaction $v_{\text{c}}(1, 2) = \delta(t_1 - t_2)/|\mathbf{r}_1 - \mathbf{r}_2|$, and the exchange-correlation potential up to second order is written as

$$V_{\text{xc}}(1) = \int_0^1 f_{\text{xc}}(1, 2) \rho(2) d2 + \int \int_0^1 g_{\text{xc}}(1, 2, 3) \rho(2) \rho(3) d2 d3. \quad (\text{B.5})$$

Applying now the chain rule in the definition of the many-body density response functions and taking into account the definition of the independent-particle density response function as well as the relation between the total and external potentials, one arrives to Eqs. 2 and 1 at first and second order, respectively.

B.2 Time-dependent current-density functional theory

TDCDFT follows the same basics as TDDFT, but the difference is that we are now interested in the microscopic response of the current-density to an externally applied time-dependent electric field, in the case of the many-body system, or to the total time-dependent electric field, in the case of the independent-particle system. From the mathematical point of view, this change of paradigm means that we are no longer interested in scalar quantities, but in vectors and tensors. In this way, up to second order, the time-dependent current-density response can be written as

$$\mathbf{j}(1) = \int_0^1 \boldsymbol{\sigma}_1(1, 2) \mathbf{E}_{\text{ext}}(2) d2 + \int \int_0^1 \boldsymbol{\sigma}_2(1, 2, 3) \mathbf{E}_{\text{ext}}(2) \mathbf{E}_{\text{ext}}(3) d2 d3, \quad (\text{B.6})$$

or alternatively as

$$\mathbf{j}(1) = \int_0^1 \boldsymbol{\sigma}_1^0(1, 2) \mathbf{E}_{\text{tot}}(2) d2 + \int \int_0^1 \boldsymbol{\sigma}_2^0(1, 2, 3) \mathbf{E}_{\text{tot}}(2) \mathbf{E}_{\text{tot}}(3) d2 d3, \quad (\text{B.7})$$

where $\boldsymbol{\sigma}_n$ and $\boldsymbol{\sigma}_n^0$ are the many-body and independent-particle current-density response tensors at n -th order, and the total electric field is related to the external electric field as

$$\mathbf{E}_{\text{tot}}(\mathbf{r}, t) = \mathbf{E}_{\text{ext}}(\mathbf{r}, t) + \mathbf{E}_{\text{H}}(\mathbf{r}, t) + \mathbf{E}_{\text{xc}}(\mathbf{r}, t). \quad (\text{B.8})$$

The Hartree electric field as a function of the current-density response is given by

$$\mathbf{E}_H(1) = \int_0^1 \mathbf{K}_H(1, 2) \mathbf{j}(2) d2, \quad (\text{B.9})$$

where \mathbf{K}_H is the tensorial Hartree kernel, which represents the tensor extension of the Coulomb interaction. In turn, the exchange-correlation electric field up to second order is written as

$$\mathbf{E}_{xc}(1) = \int_0^1 \mathbf{F}_{xc}(1, 2) \mathbf{j}(2) d2 + \int \int_0^1 \mathbf{G}_{xc}(1, 2, 3) \mathbf{j}(2) \mathbf{j}(3) d2 d3, \quad (\text{B.10})$$

with \mathbf{F}_{xc} and \mathbf{G}_{xc} the linear and quadratic tensorial exchange-correlation kernels, respectively, which can also be viewed as the tensor extension of f_{xc} and g_{xc} .

As for the density response, applying the chain rule in the definition of the many-body current-density response tensors and taking into account the definition of the independent-particle current-density response tensors as well as the relation between the total and external electric fields, the Dyson-like linear and quadratic current-density response equations are derived,

$$\sigma_1(1, 2) = \int \sigma_1^0(1, 3) \boldsymbol{\varepsilon}^{-1}(3, 2) d2, \quad (\text{B.11})$$

with $\boldsymbol{\varepsilon}^{-1}(1, 2) = \mathbf{1} + \int \mathbf{F}_{xc}(1, 3) \boldsymbol{\sigma}(3, 2) d3$ the inverse of the dielectric tensor, and

$$\begin{aligned} \sigma_2(1, 2, 3) = \int \int \int & [\boldsymbol{\varepsilon}^{-1, T}(1, 4) \sigma_2^0(4, 5, 6) \boldsymbol{\varepsilon}^{-1}(5, 2) \boldsymbol{\varepsilon}^{-1}(6, 3) \\ & + \sigma_1^T(1, 4) \mathbf{G}_{xc}(4, 5, 6) \sigma_1(5, 2) \sigma_1(6, 3)] d4 d5 d6, \end{aligned} \quad (\text{B.12})$$

respectively. As can be seen directly, Eqs. B.11 and B.12 are nothing but the tensor extension of Eqs. 2 and 1.

B.3 TDCDFT in the optical and long-wavelength limit

Since we are interested in optical responses, it is convenient to adapt TDCDFT equations to the optical and long-wavelength limit, which assumes that the microscopic response remains constant in the length-scale of the crystal's unit cell.

Regarding the Hartree contribution, the TDDFT Hartree potential is defined in Eq. B.4, while the TDCDFT Hartree electric field is defined by Eq. B.9. With the aid of Maxwell's equation $\mathbf{E}(\mathbf{r}, t) = -\nabla V(\mathbf{r}, t)$ and the continuity equation $\nabla \cdot \mathbf{j}(\mathbf{r}, t) = -\partial_t \rho(\mathbf{r}, t)$, one can reformulate the TDCDFT Hartree electric field in the wave-vector and frequency space starting from the TDDFT Hartree potential and compare it with its original definition. In this way, the tensorial Hartree kernel can be expressed as

$$\mathbf{K}_H(\mathbf{q}_1, \mathbf{q}_2, \omega) = \frac{4\pi}{i\omega} \delta_{\mathbf{q}_1 \mathbf{q}_2} \frac{\mathbf{q}_1 \odot \mathbf{q}_2}{|\mathbf{q}_1| |\mathbf{q}_2|}, \quad (\text{B.13})$$

where \mathbf{q}_n represents the crystal momentum transfer of the n -th particle. In the optical limit, *i.e.* $\lim \mathbf{q}_n \rightarrow 0$, the tensorial Hartree kernel reads then

$$\mathbf{K}_H(\omega) = \frac{4\pi}{i\omega} \mathbf{1}. \quad (\text{B.14})$$

With respect to the exchange-correlation terms, we assume that the nonlocal long-range contribution (LRC) dominates over all other terms in the optical limit. In this way, excitonic

and trionic effects in the optical limit within TDDFT are included by means of *exact* behaviors of the linear and quadratic xc kernels $\lim_{q_n \rightarrow 0} f_{xc}(\mathbf{q}_1, \mathbf{q}_2, \omega) = -A_{\text{LRC}}(\omega)/q^2$ [71] and $\lim_{q_n} g_{xc}(\mathbf{q}_1, \mathbf{q}_2, \mathbf{q}_3, \omega_1, \omega_2) = B_{\text{LRC}}(\omega_1, \omega_2)/q^3$ [23], respectively. Both limits are derived from the first-order BSE two-particle and second-order BSE three-particle correlation functions within MBPT, respectively. Following the same procedure used for the optical tensorial Hartree kernel, we also derive the expressions of the linear and quadratic tensorial exchange-correlation kernels in the optical limit, which reads as

$$\mathbf{F}_{xc}(\omega) = -\frac{A_{\text{LRC}}(\omega)}{i\omega}, \quad (\text{B.15})$$

and

$$\mathbf{G}_{xc}(\omega_1, \omega_2) = \frac{B_{\text{LRC}}(\omega_1, \omega_2)}{i\omega_1\omega_2}, \quad (\text{B.16})$$

respectively. Thus, taking into account these definitions, one can already write the Dyson-like linear and quadratic current-density response equations in the optical limit as

$$\boldsymbol{\sigma}_1(\omega) = \boldsymbol{\sigma}_1^0(\omega)\boldsymbol{\varepsilon}^{-1}(\omega), \quad (\text{B.17})$$

with $\boldsymbol{\varepsilon}^{-1}(\omega) = \mathbb{1} + \frac{4\pi-A_{\text{LRC}}(\omega)}{i\omega}\boldsymbol{\sigma}_1(\omega)$ the inverse of the optical dielectric tensor, and

$$\begin{aligned} \boldsymbol{\sigma}_2(\omega_1, \omega_2) = & \boldsymbol{\varepsilon}^{-1,T}(\omega_1 + \omega_2)\boldsymbol{\sigma}_2^0(\omega_1, \omega_2)\boldsymbol{\varepsilon}^{-1}(\omega_1)\boldsymbol{\varepsilon}^{-1}(\omega_2) \\ & + \boldsymbol{\sigma}_1^T(\omega_1 + \omega_2)\frac{B_{\text{LRC}}(\omega_1, \omega_2)}{i\omega_1\omega_2}\boldsymbol{\sigma}_1(\omega_1)\boldsymbol{\sigma}_1(\omega_2), \end{aligned} \quad (\text{B.18})$$

respectively. Here, the advantage of using TDCDFT in the optical limit becomes evident, as one obtains current-density response equations that are independent of the wave vector, in contrast to the divergences that arise in density-based response functions within TDDFT in the optical limit. Nevertheless, divergences related to the frequency are still present. These are especially cumbersome for semiconductors, which present zero conductivity as the frequency goes to zero, leading to an indeterminate form of 0/0.

In this case, the response equations can be reformulated as a function of the polarization density instead of the current density. The optical polarization-density response with respect to the many-body system and to the independent-particle system is described as

$$\mathbf{p}(\omega = \omega_1 + \omega_2) = \boldsymbol{\alpha}_1(\omega)\mathbf{E}_{\text{ext}}(\omega) + \boldsymbol{\alpha}_2(\omega_1, \omega_2)\mathbf{E}_{\text{ext}}(\omega_1)\mathbf{E}_{\text{ext}}(\omega_2), \quad (\text{B.19})$$

and

$$\mathbf{p}(\omega = \omega_1 + \omega_2) = \boldsymbol{\alpha}_1^0(\omega)\mathbf{E}_{\text{tot}}(\omega) + \boldsymbol{\alpha}_2^0(\omega_1, \omega_2)\mathbf{E}_{\text{tot}}(\omega_1)\mathbf{E}_{\text{tot}}(\omega_2), \quad (\text{B.20})$$

respectively, where $\boldsymbol{\alpha}_n$ and $\boldsymbol{\alpha}_n^0$ are the many-body and independent-particle polarizability tensors at n -th order, respectively. In the absence of magnetization and free charge and current densities, the current and polarization-density vectors are related by $\mathbf{j}(\mathbf{r}, t) = \partial_t \mathbf{p}(\mathbf{r}, t)$. This implies that conductivity and polarizability tensors in the frequency domain are related in such a way that

$$\boldsymbol{\sigma}_1^{(0)}(\omega) = -i\omega\boldsymbol{\alpha}_1^{(0)}(\omega), \quad (\text{B.21})$$

and

$$\boldsymbol{\sigma}_2^{(0)}(\omega_1, \omega_2) = -i(\omega_1 + \omega_2)\boldsymbol{\alpha}_2^{(0)}(\omega_1, \omega_2), \quad (\text{B.22})$$

at first and second order, respectively. Making the pertinent substitutions, we finally write the Dyson-like linear and quadratic optical polarization-density response equations as

$$\boldsymbol{\alpha}_1(\omega) = \boldsymbol{\alpha}_1^0(\omega)\boldsymbol{\varepsilon}^{-1}(\omega), \quad (\text{B.23})$$

with $\boldsymbol{\varepsilon}^{-1}(\omega) = \mathbb{1} - [4\pi - \mathbf{A}_{\text{LRC}}(\omega)]\boldsymbol{\alpha}_1(\omega)$ the inverse of the optical dielectric tensor, and

$$\begin{aligned} \boldsymbol{\alpha}_2(\omega_1, \omega_2) = & \boldsymbol{\varepsilon}^{-1,T}(\omega_1 + \omega_2)\boldsymbol{\alpha}_2^0(\omega_1, \omega_2)\boldsymbol{\varepsilon}^{-1}(\omega_1)\boldsymbol{\varepsilon}^{-1}(\omega_2) \\ & + i\boldsymbol{\alpha}_1^T(\omega_1 + \omega_2)\mathbf{B}_{\text{LRC}}(\omega_1, \omega_2)\boldsymbol{\alpha}_1(\omega_1)\boldsymbol{\alpha}_1(\omega_2), \end{aligned} \quad (\text{B.24})$$

respectively, free of any kind of divergence as can be seen. Hence, these are the equations we use in this work in order to account for many-body effects within the optical response up to second order at the microscopic level.

B.4 From microscopic to macroscopic optical response

The ultimate goal of this work is thus to calculate the macroscopic optical susceptibility tensor from first principles and compare it with experiment. This is done by performing a macroscopic average of the interacting optical polarizability tensor at the microscopic level given by Eqs. B.23 and B.24 [48]. In atomic units, this task is done by means of the following expressions for first and second order,

$$\boldsymbol{\chi}_1(\omega) = 4\pi\boldsymbol{\alpha}_1(\omega)\boldsymbol{\varepsilon}_M(\omega) \quad (\text{B.25})$$

and

$$\boldsymbol{\chi}_2(\omega_1, \omega_2) = 4\pi\boldsymbol{\varepsilon}_M(\omega_1 + \omega_2)\boldsymbol{\alpha}_2(\omega_1, \omega_2)\boldsymbol{\varepsilon}_M(\omega_1)\boldsymbol{\varepsilon}_M(\omega_2), \quad (\text{B.26})$$

respectively, where the macroscopic optical dielectric tensor is given by

$$\boldsymbol{\varepsilon}_M(\omega) = [\mathbb{1} - 4\pi\boldsymbol{\alpha}_1(\omega)]^{-1}. \quad (\text{B.27})$$

References

- [1] R. Boyd and D. Prato, *Nonlinear Optics*, Elsevier Science, ISBN 9780080485966 (2008).
- [2] P. A. Franken, A. E. Hill, C. W. Peters and G. Weinreich, *Generation of optical harmonics*, Phys. Rev. Lett. **7**, 118 (1961), doi:[10.1103/PhysRevLett.7.118](https://doi.org/10.1103/PhysRevLett.7.118).
- [3] B. I. Sturman and V. M. Fridkin, *The photovoltaic and photorefractive effects in noncentrosymmetric materials*, Gordon and Breach Science Publishers Philadelphia, Philadelphia (1992).
- [4] J. E. Spanier, V. M. Fridkin, A. M. Rappe, A. R. Akbashev, A. Polemi, Y. Qi, Z. Gu, S. M. Young, C. J. Hawley, D. Imbrenda, G. Xiao, A. L. Bennett-Jackson *et al.*, *Power conversion efficiency exceeding the shockley–queisser limit in a ferroelectric insulator*, Nature Photonics **10**(9), 611 (2016), doi:[10.1038/nphoton.2016.143](https://doi.org/10.1038/nphoton.2016.143).
- [5] L. Wu, S. Patankar, T. Morimoto, N. L. Nair, E. Thewalt, A. Little, J. G. Analytis, J. E. Moore and J. Orenstein, *Giant anisotropic nonlinear optical response in transition metal mononictide weyl semimetals*, Nature Physics **13**(4), 350 (2017), doi:[10.1038/nphys3969](https://doi.org/10.1038/nphys3969).
- [6] S. Patankar, L. Wu, B. Lu, M. Rai, J. D. Tran, T. Morimoto, D. E. Parker, A. G. Grushin, N. L. Nair, J. G. Analytis, J. E. Moore, J. Orenstein *et al.*, *Resonance-enhanced optical nonlinearity in the weyl semimetal taas*, Phys. Rev. B **98**, 165113 (2018), doi:[10.1103/PhysRevB.98.165113](https://doi.org/10.1103/PhysRevB.98.165113).
- [7] G. B. Osterhoudt, L. K. Diebel, M. J. Gray, X. Yang, J. Stanco, X. Huang, B. Shen, N. Ni, P. J. W. Moll, Y. Ran and K. S. Burch, *Colossal mid-infrared bulk photovoltaic effect in a type-i weyl semimetal*, Nature Materials **18**(5), 471 (2019), doi:[10.1038/s41563-019-0297-4](https://doi.org/10.1038/s41563-019-0297-4).

-
- [8] J. Ma, Q. Gu, Y. Liu, J. Lai, P. Yu, X. Zhuo, Z. Liu, J.-H. Chen, J. Feng and D. Sun, *Nonlinear photoresponse of type-ii weyl semimetals*, Nature Materials **18**(5), 476 (2019), doi:[10.1038/s41563-019-0296-5](https://doi.org/10.1038/s41563-019-0296-5).
- [9] Z. Ni, B. Xu, M.-Á. Sánchez-Martínez, Y. Zhang, K. Manna, C. Bernhard, J. W. F. Venderbos, F. de Juan, C. Felser, A. G. Grushin and L. Wu, *Linear and nonlinear optical responses in the chiral multifold semimetal rhsi*, npj Quantum Materials **5**(1), 96 (2020), doi:[10.1038/s41535-020-00298-y](https://doi.org/10.1038/s41535-020-00298-y).
- [10] T. Morimoto and N. Nagaosa, *Topological nature of nonlinear optical effects in solids*, Science Advances **2**(5), e1501524 (2016), doi:[10.1126/sciadv.1501524](https://doi.org/10.1126/sciadv.1501524), <https://www.science.org/doi/pdf/10.1126/sciadv.1501524>.
- [11] E. Luppi and V. Véniard, *A review of recent theoretical studies in nonlinear crystals: towards the design of new materials*, Semiconductor Science and Technology **31**(12), 123002 (2016), doi:[10.1088/0268-1242/31/12/123002](https://doi.org/10.1088/0268-1242/31/12/123002).
- [12] S. M. Young and A. M. Rappe, *First principles calculation of the shift current photovoltaic effect in ferroelectrics*, Phys. Rev. Lett. **109**, 116601 (2012), doi:[10.1103/PhysRevLett.109.116601](https://doi.org/10.1103/PhysRevLett.109.116601).
- [13] B. M. Fregoso, R. A. Muniz and J. E. Sipe, *Jerk current: A novel bulk photovoltaic effect*, Phys. Rev. Lett. **121**, 176604 (2018), doi:[10.1103/PhysRevLett.121.176604](https://doi.org/10.1103/PhysRevLett.121.176604).
- [14] B. M. Fregoso, *Bulk photovoltaic effects in the presence of a static electric field*, Phys. Rev. B **100**, 064301 (2019), doi:[10.1103/PhysRevB.100.064301](https://doi.org/10.1103/PhysRevB.100.064301).
- [15] S. R. Panday, S. Barraza-Lopez, T. Rangel and B. M. Fregoso, *Injection current in ferroelectric group-iv monochalcogenide monolayers*, Phys. Rev. B **100**, 195305 (2019), doi:[10.1103/PhysRevB.100.195305](https://doi.org/10.1103/PhysRevB.100.195305).
- [16] A. R. Puente-Uriona, S. S. Tsirkin, I. Souza and J. Ibañez Azpiroz, *Ab initio study of the nonlinear optical properties and dc photocurrent of the weyl semimetal tairte₄*, Phys. Rev. B **107**, 205204 (2023), doi:[10.1103/PhysRevB.107.205204](https://doi.org/10.1103/PhysRevB.107.205204).
- [17] J. Sivianes, P. Garcia-Goiricelaya, D. Hernangómez-Pérez and J. Ibañez Azpiroz, *Surface-state engineering for generation of nonlinear charge and spin photocurrents*, Phys. Rev. Lett. **135**, 256201 (2025), doi:[10.1103/h8rp-rtn8](https://doi.org/10.1103/h8rp-rtn8).
- [18] R. Martin, L. Reining and D. Ceperley, *Interacting Electrons*, Cambridge University Press, ISBN 9780521871501 (2016).
- [19] J. Deslippe, S. Louie and A. Rahman, *Ab initio theories of the structural, electronic, and optical properties of semiconductors: Bulk crystals to nanostructures*, In *Reference Module in Materials Science and Materials Engineering*. Elsevier, ISBN 978-0-12-803581-8, doi:<https://doi.org/10.1016/B978-0-12-803581-8.00764-5> (2016).
- [20] X. Liu, Q. Guo and J. Qiu, *Emerging low-dimensional materials for nonlinear optics and ultrafast photonics*, Advanced Materials **29**(14), 1605886 (2017), doi:<https://doi.org/10.1002/adma.201605886>, <https://advanced.onlinelibrary.wiley.com/doi/pdf/10.1002/adma.201605886>.
- [21] E. Runge and E. K. U. Gross, *Density-functional theory for time-dependent systems*, Phys. Rev. Lett. **52**, 997 (1984), doi:[10.1103/PhysRevLett.52.997](https://doi.org/10.1103/PhysRevLett.52.997).

-
- [22] E. K. U. Gross, J. F. Dobson and M. Petersilka, *Density functional theory of time-dependent phenomena*, pp. 81–172, Springer Berlin Heidelberg, Berlin, Heidelberg, ISBN 978-3-540-49946-6, doi:[10.1007/BFb0016643](https://doi.org/10.1007/BFb0016643) (1996).
- [23] H. Hübener, *Second-order response bethe-salpeter equation*, Phys. Rev. A **83**, 062122 (2011), doi:[10.1103/PhysRevA.83.062122](https://doi.org/10.1103/PhysRevA.83.062122).
- [24] J. Frenkel, *On the transformation of light into heat in solids. i*, Phys. Rev. **37**, 17 (1931), doi:[10.1103/PhysRev.37.17](https://doi.org/10.1103/PhysRev.37.17).
- [25] E. F. Gross, *Excitons and their motion in crystal lattices*, Soviet Physics Uspekhi **5**, 195 (1962), doi:[10.1070/PU1962v005n02ABEH003407](https://doi.org/10.1070/PU1962v005n02ABEH003407), [Usp. Fiz. Nauk **76**, 433-466 (1962)].
- [26] L. V. Keldysh and A. N. Kozlov, *Collective properties of excitons in semiconductors*, Soviet Physics JETP **27**, 521 (1968), doi:https://doi.org/10.1142/9789811279461_0011, [Zh. Eksp. Teor. Fiz. **54**,978-993 (1968)].
- [27] K. Kheng, R. T. Cox, M. Y. d' Aubigné, F. Bassani, K. Saminadayar and S. Tatarenko, *Observation of negatively charged excitons x^- in semiconductor quantum wells*, Phys. Rev. Lett. **71**, 1752 (1993), doi:[10.1103/PhysRevLett.71.1752](https://doi.org/10.1103/PhysRevLett.71.1752).
- [28] E. K. Chang, E. L. Shirley and Z. H. Levine, *Excitonic effects on optical second-harmonic polarizabilities of semiconductors*, Phys. Rev. B **65**, 035205 (2001), doi:[10.1103/PhysRevB.65.035205](https://doi.org/10.1103/PhysRevB.65.035205).
- [29] R. Leitsmann, W. G. Schmidt, P. H. Hahn and F. Bechstedt, *Second-harmonic polarizability including electron-hole attraction from band-structure theory*, Phys. Rev. B **71**, 195209 (2005), doi:[10.1103/PhysRevB.71.195209](https://doi.org/10.1103/PhysRevB.71.195209).
- [30] M. Grüning and C. Attaccalite, *Second harmonic generation in h-bn and mos₂ monolayers: Role of electron-hole interaction*, Phys. Rev. B **89**, 081102 (2014), doi:[10.1103/PhysRevB.89.081102](https://doi.org/10.1103/PhysRevB.89.081102).
- [31] M. Grüning and C. Attaccalite, *Erratum: Second harmonic generation in h-bn and mos₂ monolayers: Role of electron-hole interaction [phys. rev. b 89, 081102(r) (2014)]*, Phys. Rev. B **90**, 199901 (2014), doi:[10.1103/PhysRevB.90.199901](https://doi.org/10.1103/PhysRevB.90.199901).
- [32] M. L. Trolle, G. Seifert and T. G. Pedersen, *Theory of excitonic second-harmonic generation in monolayer mos₂*, Phys. Rev. B **89**, 235410 (2014), doi:[10.1103/PhysRevB.89.235410](https://doi.org/10.1103/PhysRevB.89.235410).
- [33] T. G. Pedersen, *Intraband effects in excitonic second-harmonic generation*, Phys. Rev. B **92**, 235432 (2015), doi:[10.1103/PhysRevB.92.235432](https://doi.org/10.1103/PhysRevB.92.235432).
- [34] A. Riefer and W. G. Schmidt, *Solving the bethe-salpeter equation for the second-harmonic generation in zn chalcogenides*, Phys. Rev. B **96**, 235206 (2017), doi:[10.1103/PhysRevB.96.235206](https://doi.org/10.1103/PhysRevB.96.235206).
- [35] A. Taghizadeh and T. G. Pedersen, *Gauge invariance of excitonic linear and nonlinear optical response*, Phys. Rev. B **97**, 205432 (2018), doi:[10.1103/PhysRevB.97.205432](https://doi.org/10.1103/PhysRevB.97.205432).
- [36] R. Fei, L. Z. Tan and A. M. Rappe, *Shift-current bulk photovoltaic effect influenced by quasiparticle and exciton*, Phys. Rev. B **101**, 045104 (2020), doi:[10.1103/PhysRevB.101.045104](https://doi.org/10.1103/PhysRevB.101.045104).

-
- [37] S. Konabe, *Exciton effect on shift current in single-walled boron-nitride nanotubes*, Phys. Rev. B **103**, 075402 (2021), doi:[10.1103/PhysRevB.103.075402](https://doi.org/10.1103/PhysRevB.103.075402).
- [38] Z. Dai and A. M. Rappe, *First-principles calculation of ballistic current from electron-hole interaction*, Phys. Rev. B **104**, 235203 (2021), doi:[10.1103/PhysRevB.104.235203](https://doi.org/10.1103/PhysRevB.104.235203).
- [39] Y. Chan, D. Y. Qiu, F. H. d. Jornada and S. G. Louie, *Giant exciton-enhanced shift currents and direct current conduction with subbandgap photo excitations produced by many-electron interactions*, Proceedings of the National Academy of Sciences **118** (2021), doi:[10.1073/pnas.1906938118](https://doi.org/10.1073/pnas.1906938118).
- [40] Y.-S. Huang, Y.-H. Chan and G.-Y. Guo, *Large shift currents via in-gap and charge-neutral excitons in a monolayer and nanotubes of bn*, Phys. Rev. B **108**, 075413 (2023), doi:[10.1103/PhysRevB.108.075413](https://doi.org/10.1103/PhysRevB.108.075413).
- [41] J. Ruan, Y.-H. Chan and S. G. Louie, *Exciton enhanced nonlinear optical responses in monolayer h-bn and mos2: Insight from first-principles exciton-state coupling formalism and calculations*, Nano Letters **24**(49), 15533 (2024), doi:[10.1021/acs.nanolett.4c03434](https://doi.org/10.1021/acs.nanolett.4c03434), PMID: 39556702, <https://doi.org/10.1021/acs.nanolett.4c03434>.
- [42] J. J. Esteve-Paredes, M. A. García-Blázquez, A. J. Uría-Álvarez, M. Camarasa-Gómez and J. J. Palacios, *Excitons in nonlinear optical responses: shift current in mos2 and ges monolayers*, npj Computational Materials **11**(1), 13 (2025), doi:[10.1038/s41524-024-01504-2](https://doi.org/10.1038/s41524-024-01504-2).
- [43] H. Hübener, E. Luppi and V. Vénard, *Ab initio calculation of second harmonic generation in solids*, physica status solidi (b) **247**(8), 1984 (2010), doi:<https://doi.org/10.1002/pssb.200983954>, <https://onlinelibrary.wiley.com/doi/pdf/10.1002/pssb.200983954>.
- [44] E. Luppi, H. Hübener and V. Vénard, *Communications: Ab initio second-order nonlinear optics in solids*, The Journal of Chemical Physics **132**(24), 241104 (2010), doi:[10.1063/1.3457671](https://doi.org/10.1063/1.3457671), https://pubs.aip.org/aip/jcp/article-pdf/doi/10.1063/1.3457671/16122687/241104_1_online.pdf.
- [45] E. Luppi, H. Hübener and V. Vénard, *Ab initio second-order nonlinear optics in solids: Second-harmonic generation spectroscopy from time-dependent density-functional theory*, Phys. Rev. B **82**, 235201 (2010), doi:[10.1103/PhysRevB.82.235201](https://doi.org/10.1103/PhysRevB.82.235201).
- [46] H. Hübener, E. Luppi and V. Vénard, *Ab initio calculation of many-body effects on the second-harmonic generation spectra of hexagonal sic polytypes*, Phys. Rev. B **83**, 115205 (2011), doi:[10.1103/PhysRevB.83.115205](https://doi.org/10.1103/PhysRevB.83.115205).
- [47] N. Gauriot, V. Vénard and E. Luppi, *Long-range corrected exchange-correlation kernels to describe excitons in second-harmonic generation*, The Journal of Chemical Physics **151**(23), 234111 (2019), doi:[10.1063/1.5126501](https://doi.org/10.1063/1.5126501), https://pubs.aip.org/aip/jcp/article-pdf/doi/10.1063/1.5126501/15567310/234111_1_online.pdf.
- [48] P. Garcia-Goiricelaya, J. Krishna and J. Ibañez Azpiroz, *Including many-body effects into the wannier-interpolated quadratic photoresponse tensor*, Phys. Rev. B **107**, 205101 (2023), doi:[10.1103/PhysRevB.107.205101](https://doi.org/10.1103/PhysRevB.107.205101).
- [49] A. Ramasubramaniam, *Large excitonic effects in monolayers of molybdenum and tungsten dichalcogenides*, Phys. Rev. B **86**, 115409 (2012), doi:[10.1103/PhysRevB.86.115409](https://doi.org/10.1103/PhysRevB.86.115409).

-
- [50] A. Molina-Sánchez, D. Sangalli, K. Hummer, A. Marini and L. Wirtz, *Effect of spin-orbit interaction on the optical spectra of single-layer, double-layer, and bulk mos₂*, Phys. Rev. B **88**, 045412 (2013), doi:[10.1103/PhysRevB.88.045412](https://doi.org/10.1103/PhysRevB.88.045412).
- [51] D. Y. Qiu, F. H. da Jornada and S. G. Louie, *Optical spectrum of mos₂: Many-body effects and diversity of exciton states*, Phys. Rev. Lett. **111**, 216805 (2013), doi:[10.1103/PhysRevLett.111.216805](https://doi.org/10.1103/PhysRevLett.111.216805).
- [52] D. Y. Qiu, F. H. da Jornada and S. G. Louie, *Screening and many-body effects in two-dimensional crystals: Monolayer mos₂*, Phys. Rev. B **93**, 235435 (2016), doi:[10.1103/PhysRevB.93.235435](https://doi.org/10.1103/PhysRevB.93.235435).
- [53] F. A. Rasmussen, P. S. Schmidt, K. T. Winther and K. S. Thygesen, *Efficient many-body calculations for two-dimensional materials using exact limits for the screened potential: Band gaps of mos₂, h-bn, and phosphorene*, Phys. Rev. B **94**, 155406 (2016), doi:[10.1103/PhysRevB.94.155406](https://doi.org/10.1103/PhysRevB.94.155406).
- [54] J. S. Ross, S. Wu, H. Yu, N. J. Ghimire, A. M. Jones, G. Aivazian, J. Yan, D. G. Mandrus, D. Xiao, W. Yao and X. Xu, *Electrical control of neutral and charged excitons in a monolayer semiconductor*, Nature Communications **4**(1), 1474 (2013), doi:[10.1038/ncomms2498](https://doi.org/10.1038/ncomms2498).
- [55] K. F. Mak, K. He, C. Lee, G. H. Lee, J. Hone, T. F. Heinz and J. Shan, *Tightly bound trions in monolayer mos₂*, Nature Materials **12**(3), 207 (2013), doi:[10.1038/nmat3505](https://doi.org/10.1038/nmat3505).
- [56] L. M. Malard, T. V. Alencar, A. P. M. Barboza, K. F. Mak and A. M. de Paula, *Observation of intense second harmonic generation from mos₂ atomic crystals*, Phys. Rev. B **87**, 201401 (2013), doi:[10.1103/PhysRevB.87.201401](https://doi.org/10.1103/PhysRevB.87.201401).
- [57] Y. J. Zhang, T. Ideue, M. Onga, F. Qin, R. Suzuki, A. Zak, R. Tenne, J. H. Smet and Y. Iwasa, *Enhanced intrinsic photovoltaic effect in tungsten disulfide nanotubes*, Nature **570**(7761), 349 (2019), doi:[10.1038/s41586-019-1303-3](https://doi.org/10.1038/s41586-019-1303-3).
- [58] J. Krishna, P. Garcia-Goiricelaya, F. de Juan and J. Ibañez Azpiroz, *Understanding the large shift photocurrent of ws₂ nanotubes: A comparative analysis with monolayers*, Phys. Rev. B **108**, 165418 (2023), doi:[10.1103/PhysRevB.108.165418](https://doi.org/10.1103/PhysRevB.108.165418).
- [59] G. Vignale and W. Kohn, *Current-dependent exchange-correlation potential for dynamical linear response theory*, Phys. Rev. Lett. **77**, 2037 (1996), doi:[10.1103/PhysRevLett.77.2037](https://doi.org/10.1103/PhysRevLett.77.2037).
- [60] G. Vignale, C. A. Ullrich and S. Conti, *Time-dependent density functional theory beyond the adiabatic local density approximation*, Phys. Rev. Lett. **79**, 4878 (1997), doi:[10.1103/PhysRevLett.79.4878](https://doi.org/10.1103/PhysRevLett.79.4878).
- [61] L. Hedin, *New method for calculating the one-particle green's function with application to the electron-gas problem*, Phys. Rev. **139**, A796 (1965), doi:[10.1103/PhysRev.139.A796](https://doi.org/10.1103/PhysRev.139.A796).
- [62] L. Hedin and S. Lundqvist, *Effects of electron-electron and electron-phonon interactions on the one-electron states of solids*, vol. 23 of *Solid State Physics*, pp. 1–181. Academic Press, doi:[https://doi.org/10.1016/S0081-1947\(08\)60615-3](https://doi.org/10.1016/S0081-1947(08)60615-3) (1970).
- [63] E. E. Salpeter and H. A. Bethe, *A relativistic equation for bound-state problems*, Phys. Rev. **84**, 1232 (1951), doi:[10.1103/PhysRev.84.1232](https://doi.org/10.1103/PhysRev.84.1232).
- [64] P. A. Young, *Lattice parameter measurements on molybdenum disulphide*, Journal of Physics D: Applied Physics **1**(7), 936 (1968), doi:[10.1088/0022-3727/1/7/416](https://doi.org/10.1088/0022-3727/1/7/416).

-
- [65] T. Sohler, M. Calandra and F. Mauri, *Density functional perturbation theory for gated two-dimensional heterostructures: Theoretical developments and application to flexural phonons in graphene*, Phys. Rev. B **96**, 075448 (2017), doi:[10.1103/PhysRevB.96.075448](https://doi.org/10.1103/PhysRevB.96.075448).
- [66] A. Molina-Sánchez and L. Wirtz, *Phonons in single-layer and few-layer mos_2 and ws_2* , Phys. Rev. B **84**, 155413 (2011), doi:[10.1103/PhysRevB.84.155413](https://doi.org/10.1103/PhysRevB.84.155413).
- [67] P. Garcia-Goiricelaya, J. Lafuente-Bartolome, I. G. Gurtubay and A. Eiguren, *Emergence of large nonadiabatic effects induced by the electron-phonon interaction on the complex vibrational quasiparticle spectrum of doped monolayer mos_2* , Phys. Rev. B **101**, 054304 (2020), doi:[10.1103/PhysRevB.101.054304](https://doi.org/10.1103/PhysRevB.101.054304).
- [68] J. Ibañez Azpiroz, S. S. Tsirkin and I. Souza, *Ab initio calculation of the shift photocurrent by wannier interpolation*, Phys. Rev. B **97**, 245143 (2018), doi:[10.1103/PhysRevB.97.245143](https://doi.org/10.1103/PhysRevB.97.245143).
- [69] G. A. Ermolaev, Y. V. Stebunov, A. A. Vyshnevyy, D. E. Tatarkin, D. I. Yakubovsky, S. M. Novikov, D. G. Baranov, T. Shegai, A. Y. Nikitin, A. V. Arsenin and V. S. Volkov, *Broadband optical properties of monolayer and bulk mos_2* , npj 2D Materials and Applications **4**(1), 21 (2020), doi:[10.1038/s41699-020-0155-x](https://doi.org/10.1038/s41699-020-0155-x).
- [70] D. J. Trainer, Y. Zhang, F. Bobba, X. Xi, S.-W. Hla and M. Iavarone, *The effects of atomic-scale strain relaxation on the electronic properties of monolayer mos_2* , ACS Nano **13**(7), 8284 (2019), doi:[10.1021/acsnano.9b03652](https://doi.org/10.1021/acsnano.9b03652), PMID: 31268680, <https://doi.org/10.1021/acsnano.9b03652>.
- [71] L. Reining, V. Olevano, A. Rubio and G. Onida, *Excitonic effects in solids described by time-dependent density-functional theory*, Phys. Rev. Lett. **88**, 066404 (2002), doi:[10.1103/PhysRevLett.88.066404](https://doi.org/10.1103/PhysRevLett.88.066404).
- [72] G. Onida, L. Reining and A. Rubio, *Electronic excitations: density-functional versus many-body green's-function approaches*, Rev. Mod. Phys. **74**, 601 (2002), doi:[10.1103/RevModPhys.74.601](https://doi.org/10.1103/RevModPhys.74.601).
- [73] F. Sottile, K. Karlsson, L. Reining and F. Aryasetiawan, *Macroscopic and microscopic components of exchange-correlation interactions*, Phys. Rev. B **68**, 205112 (2003), doi:[10.1103/PhysRevB.68.205112](https://doi.org/10.1103/PhysRevB.68.205112).
- [74] S. Botti, F. Sottile, N. Vast, V. Olevano, L. Reining, H.-C. Weissker, A. Rubio, G. Onida, R. Del Sole and R. W. Godby, *Long-range contribution to the exchange-correlation kernel of time-dependent density functional theory*, Phys. Rev. B **69**, 155112 (2004), doi:[10.1103/PhysRevB.69.155112](https://doi.org/10.1103/PhysRevB.69.155112).
- [75] Y.-M. Byun and C. A. Ullrich, *Assessment of long-range-corrected exchange-correlation kernels for solids: Accurate exciton binding energies via an empirically scaled bootstrap kernel*, Phys. Rev. B **95**, 205136 (2017), doi:[10.1103/PhysRevB.95.205136](https://doi.org/10.1103/PhysRevB.95.205136).
- [76] S. Sharma, J. K. Dewhurst, A. Sanna and E. K. U. Gross, *Bootstrap approximation for the exchange-correlation kernel of time-dependent density-functional theory*, Phys. Rev. Lett. **107**, 186401 (2011), doi:[10.1103/PhysRevLett.107.186401](https://doi.org/10.1103/PhysRevLett.107.186401).
- [77] V. U. Nazarov and G. Vignale, *Optics of semiconductors from meta-generalized-gradient-approximation-based time-dependent density-functional theory*, Phys. Rev. Lett. **107**, 216402 (2011), doi:[10.1103/PhysRevLett.107.216402](https://doi.org/10.1103/PhysRevLett.107.216402).

-
- [78] P. E. Trevisanutto, A. Terentjevs, L. A. Constantin, V. Olevano and F. D. Sala, *Optical spectra of solids obtained by time-dependent density functional theory with the jellium-with-gap-model exchange-correlation kernel*, Phys. Rev. B **87**, 205143 (2013), doi:[10.1103/PhysRevB.87.205143](https://doi.org/10.1103/PhysRevB.87.205143).
- [79] S. Rigamonti, S. Botti, V. Veniard, C. Draxl, L. Reining and F. Sottile, *Estimating excitonic effects in the absorption spectra of solids: Problems and insight from a guided iteration scheme*, Phys. Rev. Lett. **114**, 146402 (2015), doi:[10.1103/PhysRevLett.114.146402](https://doi.org/10.1103/PhysRevLett.114.146402).
- [80] J. A. Berger, *Fully parameter-free calculation of optical spectra for insulators, semiconductors, and metals from a simple polarization functional*, Phys. Rev. Lett. **115**, 137402 (2015), doi:[10.1103/PhysRevLett.115.137402](https://doi.org/10.1103/PhysRevLett.115.137402).
- [81] S. Sharma, J. K. Dewhurst, A. Sanna and E. K. U. Gross, *Comment on “estimating excitonic effects in the absorption spectra of solids: Problems and insight from a guided iteration scheme”*, Phys. Rev. Lett. **117**, 159701 (2016), doi:[10.1103/PhysRevLett.117.159701](https://doi.org/10.1103/PhysRevLett.117.159701).
- [82] S. Rigamonti, S. Botti, V. Veniard, C. Draxl, L. Reining and F. Sottile, *Rigamonti et al. reply:*, Phys. Rev. Lett. **117**, 159702 (2016), doi:[10.1103/PhysRevLett.117.159702](https://doi.org/10.1103/PhysRevLett.117.159702).
- [83] R. Del Sole, G. Adragna, V. Olevano and L. Reining, *Long-range behavior and frequency dependence of exchange-correlation kernels in solids*, Phys. Rev. B **67**, 045207 (2003), doi:[10.1103/PhysRevB.67.045207](https://doi.org/10.1103/PhysRevB.67.045207).
- [84] S. Botti, A. Fourreau, F. m. c. Nguyen, Y.-O. Renault, F. Sottile and L. Reining, *Energy dependence of the exchange-correlation kernel of time-dependent density functional theory: A simple model for solids*, Phys. Rev. B **72**, 125203 (2005), doi:[10.1103/PhysRevB.72.125203](https://doi.org/10.1103/PhysRevB.72.125203).
- [85] P. Hohenberg and W. Kohn, *Inhomogeneous electron gas*, Phys. Rev. **136**, B864 (1964), doi:[10.1103/PhysRev.136.B864](https://doi.org/10.1103/PhysRev.136.B864).
- [86] W. Kohn and L. J. Sham, *Self-consistent equations including exchange and correlation effects*, Phys. Rev. **140**, A1133 (1965), doi:[10.1103/PhysRev.140.A1133](https://doi.org/10.1103/PhysRev.140.A1133).
- [87] J. P. Perdew and A. Zunger, *Self-interaction correction to density-functional approximations for many-electron systems*, Phys. Rev. B **23**, 5048 (1981), doi:[10.1103/PhysRevB.23.5048](https://doi.org/10.1103/PhysRevB.23.5048).
- [88] P. Giannozzi, S. Baroni, N. Bonini, M. Calandra, R. Car, C. Cavazzoni, D. Ceresoli, G. L. Chiarotti, M. Cococcioni, I. Dabo, A. D. Corso, S. de Gironcoli *et al.*, *Quantum espresso: a modular and open-source software project for quantum simulations of materials*, Journal of Physics: Condensed Matter **21**(39), 395502 (2009), doi:[10.1088/0953-8984/21/39/395502](https://doi.org/10.1088/0953-8984/21/39/395502).
- [89] P. Giannozzi, O. Andreussi, T. Brumme, O. Bunau, M. B. Nardelli, M. Calandra, R. Car, C. Cavazzoni, D. Ceresoli, M. Cococcioni, N. Colonna, I. Carnimeo *et al.*, *Advanced capabilities for materials modelling with quantum espresso*, Journal of Physics: Condensed Matter **29**(46), 465901 (2017), doi:[10.1088/1361-648X/aa8f79](https://doi.org/10.1088/1361-648X/aa8f79).
- [90] P. Giannozzi, O. Baseggio, P. Bonfà, D. Brunato, R. Car, I. Carnimeo, C. Cavazzoni, S. de Gironcoli, P. Delugas, F. Ferrari Ruffino, A. Ferretti, N. Marzari *et al.*, *Quantum ESPRESSO toward the exascale*, The Journal of Chemical Physics **152**(15), 154105 (2020), doi:[10.1063/5.0005082](https://doi.org/10.1063/5.0005082).
- [91] L. Kleinman, *Relativistic norm-conserving pseudopotential*, Phys. Rev. B **21**, 2630 (1980), doi:[10.1103/PhysRevB.21.2630](https://doi.org/10.1103/PhysRevB.21.2630).

-
- [92] D. R. Hamann, *Generalized norm-conserving pseudopotentials*, Phys. Rev. B **40**, 2980 (1989), doi:[10.1103/PhysRevB.40.2980](https://doi.org/10.1103/PhysRevB.40.2980).
- [93] D. R. Hamann, *Optimized norm-conserving vanderbilt pseudopotentials*, Phys. Rev. B **88**, 085117 (2013), doi:[10.1103/PhysRevB.88.085117](https://doi.org/10.1103/PhysRevB.88.085117).
- [94] M. Schlipf and F. Gygi, *Optimization algorithm for the generation of oncv pseudopotentials*, Computer Physics Communications **196**, 36 (2015), doi:<https://doi.org/10.1016/j.cpc.2015.05.011>.
- [95] P. Scherpelz, M. Govoni, I. Hamada and G. Galli, *Implementation and validation of fully relativistic gw calculations: Spin-orbit coupling in molecules, nanocrystals, and solids*, Journal of Chemical Theory and Computation **12**(8), 3523 (2016), doi:[10.1021/acs.jctc.6b00114](https://doi.org/10.1021/acs.jctc.6b00114), PMID: 27331614.
- [96] A. Molina-Sánchez, K. Hummer and L. Wirtz, *Vibrational and optical properties of mos2: From monolayer to bulk*, Surface Science Reports **70**(4), 554 (2015), doi:<https://doi.org/10.1016/j.surfrep.2015.10.001>.
- [97] A. Marini, C. Hogan, M. Grüning and D. Varsano, *yambo: An ab initio tool for excited state calculations*, Computer Physics Communications **180**(8), 1392 (2009), doi:<https://doi.org/10.1016/j.cpc.2009.02.003>.
- [98] D. Sangalli, A. Ferretti, H. Miranda, C. Attaccalite, I. Marri, E. Cannuccia, P. Melo, M. Marsili, F. Paleari, A. Marrazzo, G. Prandini, P. Bonfà *et al.*, *Many-body perturbation theory calculations using the yambo code*, Journal of Physics: Condensed Matter **31**(32), 325902 (2019), doi:[10.1088/1361-648X/ab15d0](https://doi.org/10.1088/1361-648X/ab15d0).
- [99] B. I. Lundqvist, *Single-particle spectrum of the degenerate electron gas*, Physik der kondensierten Materie **6**(3), 193 (1967), doi:[10.1007/BF02422716](https://doi.org/10.1007/BF02422716).
- [100] B. I. Lundqvist, *Single-particle spectrum of the degenerate electron gas*, Physik der kondensierten Materie **6**(3), 206 (1967), doi:[10.1007/BF02422717](https://doi.org/10.1007/BF02422717).
- [101] A. W. Overhauser, *Simplified theory of electron correlations in metals*, Phys. Rev. B **3**, 1888 (1971), doi:[10.1103/PhysRevB.3.1888](https://doi.org/10.1103/PhysRevB.3.1888).
- [102] F. Bruneval and X. Gonze, *Accurate gw self-energies in a plane-wave basis using only a few empty states: Towards large systems*, Phys. Rev. B **78**, 085125 (2008), doi:[10.1103/PhysRevB.78.085125](https://doi.org/10.1103/PhysRevB.78.085125).
- [103] A. Guandalini, P. D'Amico, A. Ferretti and D. Varsano, *Efficient gw calculations in two dimensional materials through a stochastic integration of the screened potential*, npj Computational Materials **9**(1), 44 (2023), doi:[10.1038/s41524-023-00989-7](https://doi.org/10.1038/s41524-023-00989-7).
- [104] R. Haydock, *The recursive solution of the schrodinger equation*, vol. 35 of *Solid State Physics*, pp. 215–294. Academic Press, doi:[https://doi.org/10.1016/S0081-1947\(08\)60505-6](https://doi.org/10.1016/S0081-1947(08)60505-6) (1980).
- [105] J. E. Sipe and E. Ghahramani, *Nonlinear optical response of semiconductors in the independent-particle approximation*, Phys. Rev. B **48**, 11705 (1993), doi:[10.1103/PhysRevB.48.11705](https://doi.org/10.1103/PhysRevB.48.11705).
- [106] C. Aversa and J. E. Sipe, *Nonlinear optical susceptibilities of semiconductors: Results with a length-gauge analysis*, Phys. Rev. B **52**, 14636 (1995), doi:[10.1103/PhysRevB.52.14636](https://doi.org/10.1103/PhysRevB.52.14636).

-
- [107] J. E. Sipe and A. I. Shkrebtii, *Second-order optical response in semiconductors*, Phys. Rev. B **61**, 5337 (2000), doi:[10.1103/PhysRevB.61.5337](https://doi.org/10.1103/PhysRevB.61.5337).
- [108] G. Pizzi, V. Vitale, R. Arita, S. Blügel, F. Freimuth, G. Géranton, M. Gibertini, D. Gresch, C. Johnson, T. Koretsune, J. Ibañez-Azpiroz, H. Lee *et al.*, *Wannier90 as a community code: new features and applications*, Journal of Physics: Condensed Matter **32**(16), 165902 (2020), doi:[10.1088/1361-648x/ab51ff](https://doi.org/10.1088/1361-648x/ab51ff).
- [109] Y.-h. Chan, J. B. Haber, M. H. Naik, J. B. Neaton, D. Y. Qiu, F. H. da Jornada and S. G. Louie, *Exciton lifetime and optical line width profile via exciton–phonon interactions: Theory and first-principles calculations for monolayer mos2*, Nano Letters **23**(9), 3971 (2023), doi:[10.1021/acs.nanolett.3c00732](https://doi.org/10.1021/acs.nanolett.3c00732), PMID: 37071728, <https://doi.org/10.1021/acs.nanolett.3c00732>.